Soft Matter

PAPER

Cite this: *Soft Matter*, 2022, **18**, 2767

Combing a double helix†

Thomas B. Plumb-Reyes,[a] Nicholas Charles[a] and L. Mahadevan *[b]

Received 26th October 2021,
Accepted 18th February 2022

DOI: 10.1039/d1sm01533h

rsc.li/soft-matter-journal

Combing hair involves brushing away the topological tangles in a collective curl, defined as a bundle of interacting elastic filaments. Using a combination of experiment and computation, we study this problem that naturally links topology, geometry and mechanics. Observations show that the dominant interactions in hair are those of a two-body nature, corresponding to a braided homochiral double helix. This minimal model allows us to study the detangling of an elastic double helix driven by a single stiff tine that moves along it and leaves two untangled filaments in its wake. Our results quantify how the mechanics of detangling correlates with the dynamics of a topological quantity, the link density, that propagates ahead of the tine and flows out the free end as a link current. This in turn provides a measure of the maximum characteristic length of a single combing stroke in the many-body problem on a head of hair, producing an optimal combing strategy that balances trade-offs between comfort, efficiency and speed of combing in hair curls of varying geometrical and topological complexity.

Introduction

Long-haired people are familiar with a well-known strategy for combing their hair: comb away the tangles starting close to the free hair ends, and work steadily upward towards the scalp. This allows for the untangling of a collective curl—a bundle of interacting elastic filaments clamped at one end, free at the other, and braided and tangled in between—to proceed more efficiently from the free end, minimizing pain but at the expense of time. But how does a comb work its way through a curl? This quotidian problem which lies at the intersection of mechanics, geometry and topology has many cousins—the carding of textiles and felts,[1,2] and the spontaneous tangling and detangling of polymers in a flow,[3,4] of flux lines in superconductors[5] and of magnetic fields in solar coronae[6] among other problems. In the context of hair, there has been a recent resurgence of interest in characterizing the effective properties of fiber assemblies and packings,[7–14] inspired by technological applications to fields such as robotics, and the computer animation of hair *etc.*[15,16] However, most of these studies neglect individual hair–hair interactions, and little is known about the dynamics of detangling in complex packings of fibers and hair from a mechanical, geometrical or topological point of view.

Minimal model of hair curl

The complexity of detangling hair physically is matched by the difficulty of a physical and mathematical description of the combing problem. This is because of the many-body nature of interacting filaments (hairs) and their potential for long-range interactions; interactions at one location along the curl affect interactions elsewhere by preventing the hairs from sliding relative to each other, moving past each other *etc.* Indeed, this is similar to what is seen in entangled polymer melts and other thermal analogs that have been studied for a long time[17] (note that our use of ''interaction'' is similar to the concept of ''entanglement'' in polymer physics), with one critical difference – polymers are subject to thermal (Brownian) fluctuations owing to their small size while hairs are effectively at zero temperature. In Fig. 1a, we see an example of a curl of horsehair that is gently entangled near the free end, tightly packed near the other end, and braided along its bulk. To quantify the nature of these interactions, we digitally color each strand in images of a curl of hair by first segmenting it into sections (Fig. 1b), and then count and characterize the internal interactions of each strand using the definitions in Fig. 1c. Viewing the curl by projecting it onto a plane parallel to the main axis, we define an interaction to be where strands cross each other, but ignoring the sign of the crossing, so that our metric acts as an upper bound on the true number of signed interactions. Because hair entanglements can be removed through the free end during each combing stroke, it is not relevant to count interactions over the whole length of the curl. Instead it suffices to consider a scale comparable to the smaller of two natural scales: the natural radius of curvature or the length determined

[a] *School of Engineering and Applied Sciences, Harvard University, Cambridge, MA 02138, USA*

[b] *School of Engineering and Applied Sciences, Departments of Physics and Organismic and Evolutionary Biology, Harvard University, Cambridge, MA, 02138, USA. E-mail: lmahadev@g.harvard.edu*

† Electronic supplementary information (ESI) available. See DOI: 10.1039/d1sm01533h

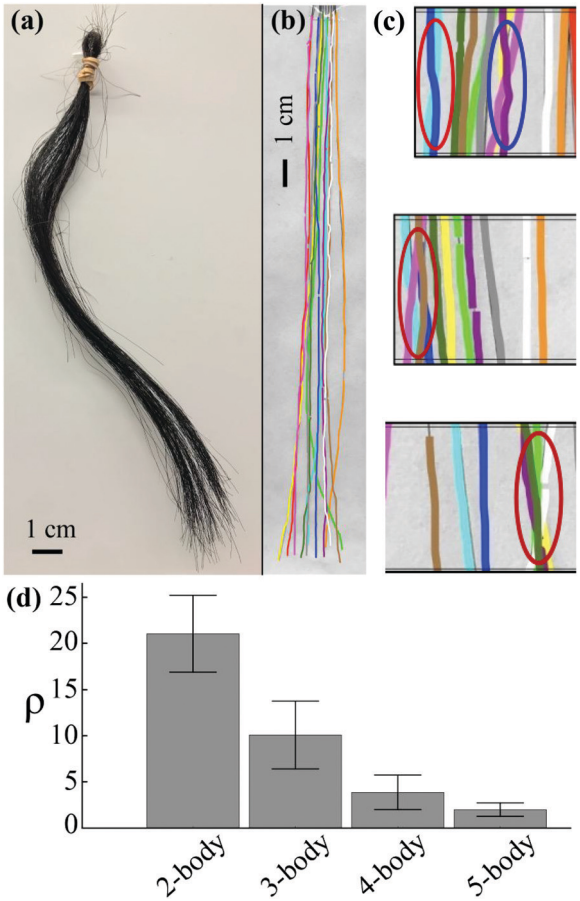

Fig. 1 Tangles in hair. (a) Curl of horse hair. (b) Colored curl of 12 human hairs, clamped at one end. (c) Examples from (b) of N-body interactions (N = 2–5 circled left to right, top to bottom). (d) Histogram of N-body interactions for a sample similar to (b) with ρ = number of interactions per unit length (in meters). We segment the curl into 20 sections, count interaction types as shown in (c) within each section and average.

by the balance between elasticity and gravity. In our study of naturally straight hair, we use the gravitational length which of order $O(10)$ cm.

In Fig. 1d, we plot the number of N–body interactions, and see that pair-wise interactions form a plurality of the tangle types (the extent to which pair-wise interactions dominate depends on curl segmentation, chosen to match the characteristic length over which hairs curl; see Appendix for details). While this plurality would likely be less pronounced for curlier hair, we restrict ourselves to relatively straight curls–*i.e.*, where an individual hair's radius of curvature is on the same order as its length. For strongly curled hair, our analysis would need to be revisited since it is likely that multi-hair interactions are far more numerous there.

Experimental observations of combing

Given the dominance of two-body interactions, we consider a minimal model of the comb-curl system: two homochiral entwined helices clamped at the top end and hanging freely at the bottom. Rather than working with hair, here we work with a simple mimic – a pair of filaments made of nylon heated to force them to conform to 3-D printed helically grooved cylinders with a constant radius and pitch, and then cooled, and entwined. This assembly is then pierced at the midpoint of the double helix centerline by a single stiff rod (the tine of a comb). As the tine moves downward quasi-statically, it detangles the downstream region of the curl. By connecting the tine to an Instron 5566 material testing machine, we measure the force-extension curves associated with the combing of a double helix.‡

In Fig. 2a we show that quasi-static combing (the physically relevant case when inertial effects are negligible) leads to a response that can be associated with unwinding the helix, kinking it or both. Unwinding causes the relative rotation of one filament endpoint around the other, but frequently leads to kinking that results from shear/sliding between the two helices and leads to a characteristically bent state (Fig. 2a and b). Additionally, we see that the filaments are slightly over-wound and compressed ahead of the tine, and under-wound and extended behind it. To examine the force-extension curves for different combing parameters, we note that the double helix can be parametrized in terms of the helix radius R and pitch P, the filament radius r, tine radius t, as shown in Fig. 2b, expressed in terms of the dimensionless ratios $\pi_1 = P/r$, $\pi_2 = R/r$ and $\pi_3 = t/r$. (See Appendix for the dependence of the force-extension curves as a function of π_3 since t appears to have little impact on the results.)

In Fig. 2d and e we show the scaled force on the tine $f = Fl_0^2/B$ as a function of the dimensionless tine displacement x (scaled by the filament radius r), where F is unscaled force, B is hair bending rigidity and l_0 is a fixed reference length§. Helices of smaller pitch and radii that are more tightly wound require larger forces to detangle, consistent with experience and intuition. In all cases, there is an initial rise in the force extension curve before a leveling off. The rise corresponds to the phenomena of overwinding of the helix in front of the tine and underwinding behind the tine, while the leveling off is associated with the tine jamming and then breaking through even as the free ends unwind. For loose helices, *i.e.* $P/r > c \approx 20$, there is no tine jamming or maximum in the force. To elucidate the force patterns unique to combing, we compare the forces required to comb a double helix with those required to stretch a single helix with the same pitch and radius (*i.e.*, a helix with initial angle $\alpha \sim P/R$ and helix radius R extended to final angle α_1 and helix radius R_1;[18] see Appendix for details). Not surprisingly, we find that the force-extension curve for combing a double helix shows a flattening (softening) in contrast with the divergent response for a single helix that is

‡ Similar force testing experiments were performed with real curls of hair (human and horse) but are not included in this publication to focus on the minimal model results.

§ Note that l_0 = 0.01m is a fixed reference length used to make quantities dimensionless and was chosen as the typical order of magnitude length over which hairs curl at their curliest location.

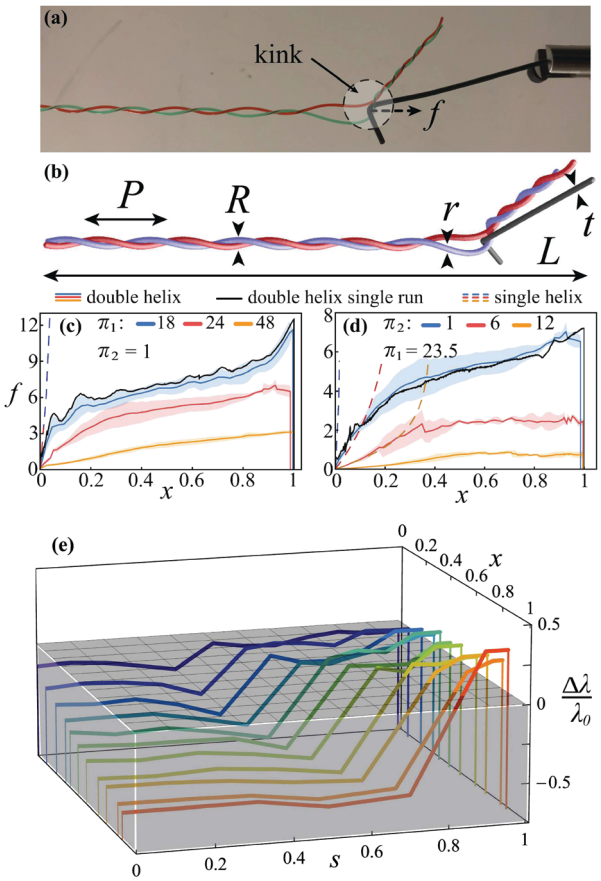

Fig. 2 Combing a double helix. (a) As the tine moves along the double helix from the clamped end towards the free end, it sometimes forms a kink about which the helix whirls as link flows out of the bundle. (b) Schematic of combing a double helix with pitch P, radius R (half the distance between individual filament centerlines), filament radius r, tine radius t and helix length L. (c and d) Scaled force $f = \frac{l_0^2 F}{B}$ applied by tine over scaled distance combed $x = \frac{d}{D}$, where F is unscaled force, d is unscaled distance combed, l_0 = 0.01m is a characteristic length, B is the single filament bending rigidity and D is total tine displacement required to detangle the helices. Dashed curves show theoretical force predicted for stretching a single helix; black curves show a single representative combing. We scan the parameter space varying (c) $\pi_1 = P/r$ and (d) $\pi_2 = R/r$. See Appendix for details and variation as a function of $\pi_3 = t/r$. (e) Change in link density $\Delta\lambda$ normalized by initial link density λ_0 as a function of dimensionless arclength $s = S/\ell$ for $\pi_1 = 18$, $\pi_2 = 1$, plotted for several normalized tine locations, showing flow of link from clamped end and eventually out of the free end. In all experiments, $r = 4.25 \times 10^{-4}$ m and helix length $L = 0.15$ m.

straightened out. This is because the moving tine untangles the two filaments, eventually decoupling the helix strands so that the force felt by the tine eventually vanishes, while the force to straighten an inextensible helix becomes large as the end-to-end distance becomes comparable to the length of the filament.

The unlinking of the homochiral helices during this process can be quantified in terms of the Calugareanu–Fuller–White (CFW) theorem[19–21] which states that $Lk = Tw + Wr$, where Link (Lk) quantifies the oriented crossing number of the two filaments averaged over all projection directions (equivalent to the Gauss Linking integral) and effectively counts the number of full turns one filament makes around the other,[22] Twist (Tw) is the integrated rotation of one filament around the two-filament-centerline, and Writhe (Wr) is related to the (negative) integral of the geometric torsion of the centerline. To quantify the topology of the double helix, we treat the two interwoven filaments as two edges of a ribbon and compute the local link and twist densities, $\lambda(S)$ and $\tau(S)$, defined as link and twist per unit length along the double helix centerline as a function of arclength S. Since Lk is a topological invariant while Tw is not, we characterize the ribbon in terms of λ. Since Lk is an inherently global quantity whereas Tw is the integral of the local twist density $\tau(S)$, τ can be defined more naturally than λ; for a relatively straight double helix, $Wr \approx 0$, allowing us to set $\lambda(S) \approx \tau(S)$.[23]

In Fig. 2e we show the evolution of the link density λ calculated from images of the helix taken as the tine moved. We see that an initially uniform $\lambda(S)$ evolves into a step-like profile as the tine induces an excess of link ahead of it and a deficit behind it, while link flows through the helical braid from the clamped towards the free end. For tine displacements $x \lesssim 0.2$, the scaled jump in the link density $\Delta\lambda/\lambda_0 > 0$ across the tine (λ_0 being the initial link density) increases faster than the rate it which is expelled from the free end. This jump eventually reaches a plateau as the tine gets closer to the free end, and then induces a uniform flux of link there that eventually unlinks the filaments.

We now turn to correlate the experimentally observed spatio-temporal evolution of link density associated with the motion of the tine to the evolution of the force on it. For a double helix that is tightly wound initially, as the tine propagates, ahead of it the scaled pitch $\pi_1 = P/r$ decreases, concomitant with the propagation of a localized jump in the link density.¶ This localized jump in the local link density causes the double helix to tighten and stiffen and eventually the tine jams. This often but not always causes the filaments to slide relative to each other, leading to a kinked configuration seen in Fig. 2a and b. As the tine breaks through, there is a simultaneous reduction in the force, before the same cycle repeats again. If a kink forms, the kinked double helix twirls about the axis of tine motion as the tine moves (see Video-S1, ESI†). If the double helix is initially loose enough, link propagates more easily from the tine location to the free end, and $\lambda(S)$ never crosses the threshold needed for kinking, so that the force required to comb does not oscillate strongly. In all cases, there is a current of link that flows out of the free end, driven by a combination of the unwinding of the free ends of the individual filaments, and the whirling rotation of the kinked portion of the double helix.

By using the local link, twist and writhe density instead of the local curvature and torsion, we can characterize the untangling of the double helix. In this picture, combing corresponds

¶ The abrupt change in link density, termed here a link front, is more visible in Fig. 3e than its experimental counterpart, since link density measurements could not be performed with as high resolution in experimental curls as in simulated ones.

topologically to a reduction in the global *Lk* driven by the flow of a link current out of the free end.

Numerical simulations of combing

To quantify our experiments on the nonlinear topological mechanics of interacting filaments, we use a numerical approach that models each hair using the Kirchhoff–Cosserat theory[24,25] and solve the equations using a numerical integration scheme.[26] In the limit of very thin filaments such as hair, the model naturally reduces to the Kirchhoff–Love theory for inextensible, unshearable filaments.[18] We define $S \in [0, \ell]$ as the material coordinate (also the arc length) of the rod of rest length ℓ, $\mathbf{r}(S)$ as the position vector of the center-line, and a triad of orthonormal directors $\mathbf{d}_1(S)$, $\mathbf{d}_2(S)$, $\mathbf{d}_3(S) = \partial_S \mathbf{r}$ that defines the cross-section orientation. Then any body-convected vector $\mathbf{v}$ with lab-frame coordinates $\bar{\mathbf{v}}$ may be written as $\mathbf{v} = \mathbf{Q}\bar{\mathbf{v}}$, where $\mathbf{Q}(s) \in SO(3)$ is a rotation matrix, and the bending and twist strain vector is given by $\kappa = \mathrm{vec}(\partial_S \mathbf{Q}^T \mathbf{Q})$. If $\mathbf{N}(S)$ is the internal force resultant, $\mathbf{f}_g$ as gravitational force density, the equilibrium equations for the filament are[25,26]

$$0 = \partial_S \mathbf{N} + \mathbf{f}_g \tag{1}$$

$$0 = \partial_S(\mathbf{B}(\kappa - \kappa_0)) + \partial_S \mathbf{r} \times \mathbf{N} \tag{2}$$

where $\mathbf{B}$ is the matrix of bending and twisting rigidities, κ_0 is the natural curvature of the unstressed filament. The associated boundary conditions of the filaments are that it is clamped at one end and free at the other. We compute equilibrium configurations by solving an overdamped version of the corresponding dynamical system, since that is the computationally most convenient method of deploying the numerical scheme.[26]

To simulate the initial state of a curl of hairs such as that depicted in Fig. 1b, we start with a collection of clamped filaments hanging in a gravitational field $|f_g| = mAg$ ($g \sim 10$ N kg^{-1}, m is the filament mass density and A is the filament cross-sectional area), resulting in a curl such as that shown in Fig. 3a. We then introduce an intrinsic curvature along the discretized filament randomly drawn from a Gaussian distribution with zero mean and variance matching the distribution of experimentally observed curvatures (see Appendix for details), shown in Fig. 1b. Finally, we let the hairs relax elastically to their new rest configurations, determined by a competition between nonzero intrinsic curvature and gravitational straightening (see Appendix). After the hairs relax, we count interactions using the same method as used in experiments, leading to the histogram of interactions per unit length shown in Fig. 3b. We find that pairwise interactions dominate, in agreement with experimental results (see Appendix where we show that these interactions do not change qualitatively in a 3d array).

To follow the combing of an elastic double helix as in Fig. 2, we start with a random distribution of initial internal strains for each of the filaments and anneal the pair into a double helix, clamped at one end and hanging freely under the influence of gravity. We then insert a rigid rod as a tine between the two helices close to the clamped end and move it quasi-statically towards the free end. As in experiments, when the tine moves toward the free end, it detangles the helices by pushing link out ahead of itself. In Fig. 3c and d we show the numerically computed force applied by the tine during combing, and see that the results are similar to our experiments shown in Fig. 2c and d.‖ Comparing the evolution of the helix topology numerically,[27] Fig. 3e shows that this also matches the experimental pattern of overwinding ahead and underwinding

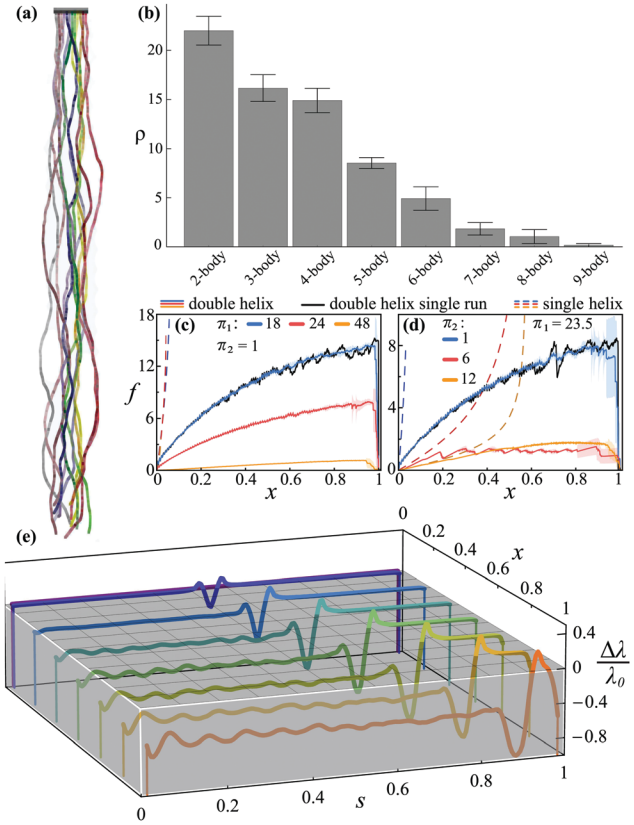

Fig. 3 Numerical results. (a) Simulated curl of 12 hairs modeling those in Fig. 1b. (b) Hair interactions as in Fig. 1d for simulations similar to (a), where ρ = number of interactions per unit length (in meters). ℓ = 0.2 m, $r = 7.5 \times 10^{-5}$ m and E = 1 GPa. See appendix for 3-dimensional curl results. (c and d) Scaled force $f = \frac{l_0^2 F}{B}$ applied by tine over scaled distance combed $x = \frac{d}{D}$, where parameters are defined as in Fig. 2. Dashed curves show theoretical force predicted for stretching single helix an equivalent distance; black curves show single representative combing. We scan the parameter space varying (c) $\pi_1 = P/r$ and (d) $\pi_2 = R/r$. See Appendix for details and variation as a function of $\pi_3 = t/r$. (e) Change in link density $\Delta\lambda$ normalized by initial link density λ_0 as a function of dimensionless arclength $s = S/\ell$ for helix with $\pi_1 = 18$, $\pi_2 = 1$, plotted for several tine locations, qualitatively reproducing experimental trends seen in Fig. 2e. See Appendix for simulation settings. Note that f, x and s are dimensionless.

‖ The high-frequency oscillations seen in the mean force curves are due to the oscillation in contact force between the tine and double helix filaments as the tine passes by each discrete node in the double helical braid.

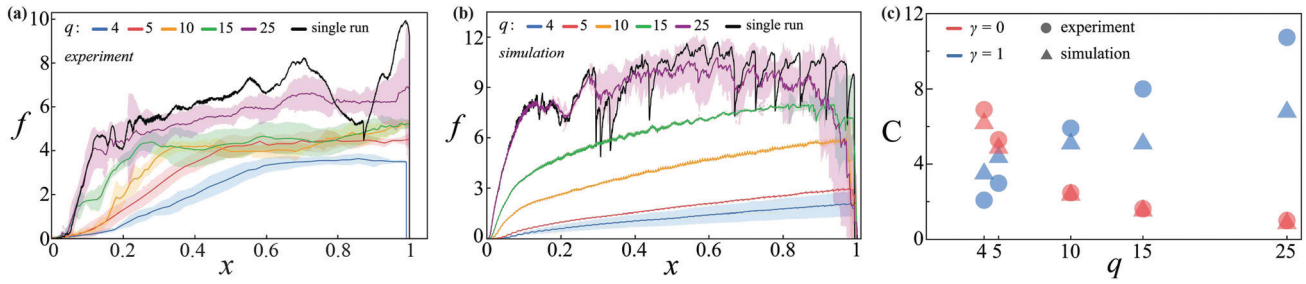

Fig. 4 (a and b) Scaled force f over scaled distance combed x for (a) experimental and (b) simulated double helices with varying number of links. Scaling of x is different for each curve since the total raw tine displacement needed to comb each curl is different. Below a certain link threshold, combing finishes without kink formation. Black curves show a single representative combing for q = 25. Filament parameters are the same as in Fig. 2. (c) Cost C to comb a 10m double helix over number of downstream pitches q detangled per combing, using the strategies shown in (a and b) – see text for details. Note that q is intrinsic to combing strategy. C combines maximum exerted force (proportional to pain felt during combing) and time required to comb; γ = 0 considers only time and corresponds to straight hair; γ = 1 considers only pain and corresponds to curly hair. Simulation and experiment how optimal combing strategy shifts depending on hair curvature.

behind the tine, shown in Fig. 2e. The oscillations in $\lambda(s)$ on the clamped side of the tine come from the periodic shearing of the clamped side filament segments with respect to each other, a phenomenon that occurs on too fine a resolution to be seen in experiments. The small discrepancies between the quantitative values observed in the numerical and experimental results may come from inhomogeneities in the geometry and material properties of the double helix in experiments. We note that the numerical calculations neglect contact friction; including contact friction in our simulations leads to force-displacement curves with similar shapes, indicating that in most situations friction effects combing quantitatively but not qualitatively.

Optimal combing strategy

Complementing our analysis of the topological mechanics of combing a double helix, we now consider how a curl's resistance to combing varies with the style of combing, *e.g.* short strokes *versus* long strokes. Noting that a single helix pitch corresponds to one helix filament revolving once around the other helix filament, we fix R/r = 1 and P/r = 24 and vary q, the number of pitches that initially separate the tine from the free end of the double helix. In experiment (Fig. 4a) and simulation (Fig. 4b) we find that significant tine jamming—as indicated by the plateaus in the force-displacement curves—occurs only when we start combing more than q = 4–5 helix pitches away from the free end**. The differences between the two sets of curves is likely due to not accounting for friction in the computations, and explains the larger number of plateaus seen in the large-q experiments relative to the more smooth force evolution seen in computations. Nevertheless, we see that starting to comb nearer to the free end allows link to be expelled more easily, leading to complete untangling before the differential link density across the tine surpasses the threshold for kink formation and jamming, consistent with experience.

To quantify this intuitive result, we define a cost $C(q)$ for combing a double helix of length L using a strategy in which the tine is repeatedly inserted q links upstream from the last insertion point and pulled through to the free end, thus detangling q links of the helix each iteration. To illustrate the trade-offs between $f_{\max}$, the maximum dimensionless force during combing, and the detangling quantized in terms of the number of strokes q_0/q needed to complete the combing process (q_0 = 25 is a fixed number of pitches characteristic to the q-values used in these combing strategies), we use the simplest linear cost that can interpolate between pain and time. Writing this cost $C(q) = \gamma f_{\max} + (1-\gamma)\frac{q_0}{q}$ (see Appendix for details), we consider the relative cost of the two effects by varying γ to optimize a combing strategy based on the initial nature of the double helix. For very curly hair, choosing $\gamma \sim O(1)$ is more sensible, while for straight hair, choosing $\gamma \sim 0$ is better. Using the results for the maximum force from Fig. 2 and 3, we calculate the cost $C(q)$ for the case of curly and straight hair. In Fig. 4c, we see that for straight hair ($\gamma \sim 0$), the cost decreases as q increases, *i.e.* the number of strokes decreases, while for curly hair ($\gamma \sim 1$), the cost is lowest for small q as it is biased to minimize the cost associated with the maximum force. We note that, while a detailed study of the effects of contact friction is beyond the scope of this work, several simulations showed that friction may change combing force-displacement curves quantitatively but not qualitatively. Hence, lubricating hair may reduce the pain felt during combing, effectively reducing the γ that should be used to compute an optimal combing strategy for a particular curl geometry.

Conclusions

Our study has shown that a first approximation to the many-body problem of combing a curl of relatively straight hair can be captured by considering the combing of a single double helix, a two-body problem with complex spatially extended

** Quantitative differences in the shape of experimental and numerical force-displacement curves in Fig. 4 likely stem from our model's neglect of contact friction.

interactions. This process connects topology, geometry and mechanics *via* a relation between flow of link driven by the tine and out of the free end, and the time-varying force felt by the tine. Our results also suggest that the two-body problem also has the ability to capture the correct optimal strategy of combing a tangle by balancing the cost of many short strokes relative to longer, potentially more painful ones. While material properties such as stiffness, friction, pretwist and cross-sectional shape would likely quantitatively impact our results, we expect the connections presented here are a start towards understanding the mechanics of combing qualitatively different styles of hair. A natural next step is to extend our combing results to real hair and account for variations in their geometric, entanglement and material properties, their strong frictional anisotropy, and the dependence of these parameters on environmental conditions such as humidity and temperature.

Conflicts of interest

There are no conflicts to declare.

Appendix

Hair curl interactions

To quantify the nature of hair–hair interactions, we segment the experimental curls into sections, and then count and characterize the internal interactions of each strand using the interaction types shown in Fig. 1c, noting that our definition of interaction is an upper bound on the true number of interactions (note that our use of ''interaction'' corresponds to ''entanglement'' in polymer physics). While the plurality of two-body interactions would give way to a predominance of many-body interactions for curlier hair, we restrict ourselves to relatively straight curls, leaving an investigation of how curliness affects hair–hair interactions to future work.

Even in this limit, the dominance of two-body interactions depends, to some degree, on the length of segment used to compartmentalize the curl. Since our goal is to investigate the local interactions making up the global tangling of the hair, we sought a segment length that would isolate local interactions—*i.e.*, those that take place over a length scale comparable to the characteristic length over which the hair curves at its curliest locations. We chose 20 segments empirically to produce a segment length roughly equal to that characteristic length.

Other curl properties, such as volumetric density of hairs in the region of space occupied by the curl, hair thickness, and average hair curvature, may also affect the precise relative abundances of N–body interactions. However, for this study, we limit ourselves to dry-combing of relatively straight hair, in an attempt to reduce the formidable complexity of the many-body problem to a more tractable two-body problem, and leaving for future work a more detailed investigation of the combing of a complete and complex curl.

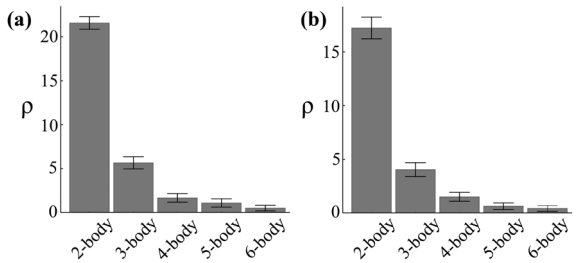

Fig. 5 Hair curl interactions in three dimensions. Histogram of hair interaction types for simulated curls similar to those used for Fig. 3b. Here, we clamp the top of the hairs in a planar triangular lattice, letting all hairs hang down in the same direction, loosely filling a volume of space below the triangular lattice. We segment the curl into 20 layers, count interaction types defined in Fig. 1c within each layer and average over all layers and curls. In three dimensions we can no longer use projected intersections to define hair interactions. In (a) we define an interaction by hairs being in contact. In (b), we use a linking number threshold to define interactions. In particular, we segment the curl into twenty segments; in any single segment, if $Lk(A, B) > m$, where A and B are the parts of two hairs which lie in the given segment, then A and B interact. We empirically determine that $m = 0.4$ is roughly the smallest linking threshold that provides nontrivial segregation of interaction types. Presumably, were m and segment length scaled equivalently, results would change only as a function of segment length, not directly as a result of changing m. Here ρ = number of interactions per unit length (in meters), and we again find pairwise interactions to be dominant. Bar height represents mean ρ while error bars show standard error in ρ.

To understand hair–hair interactions from a computational perspective, leading to Fig. 3b, we simulate twelve hairs with their top ends clamped in a planar triangular lattice. The hairs hang freely down from their clamped tops, loosely filling the volume below the triangular lattice. As with the two-dimensional array of hairs considered in Fig. 3b, we then introduce intrinsic curvature into the hairs. The random curvature at each node of each hair is sampled from a Gaussian distribution of curvatures with zero mean and standard deviation $\sim 1\ \mathrm{m}^{-1}$. This distribution was chosen to match the local curvatures of the hairs used in experiment, and was determined by sampling the local radius of curvature of several individual hairs at evenly spaced locations along the hairs. We employ two interaction criteria to determine the presence of interactions, both of which lead to similar results: in Fig. 5a, we use contact; in Fig. 5b we consider two hairs to interact within a single layer of the curl if the Lk between the segments of the two hairs within that layer is greater than a fixed threshold, here set to $Lk_{\mathrm{thresh}} = 0.4$, determined empirically to maximize intersection classification accuracy. We again find pairwise interactions to be the most prevalent, regardless of the definition of an interaction.

The qualitative similarity between Fig. 1d and 3b suggests that real hair curvatures are distributed similarly to the independently randomly sampled curvatures used in simulation. The similarity between simulated and experimental results (Fig. 1d and 3b) implies that for real hairs, there is significant

statistical independence between the local hair curvatures at points close in arclength along the same hair and equivalent points on nearby hairs. Curls of hair characterized by such independence are ''thermalized''and mimic what would be seen in a real curl.

Elasticity *versus* gravity in free-hanging hair

In Fig. 1b, we show a curl of hair used in studying hair interactions. Upon close inspection, one can see that at the bottom of this curl, the hairs are more coiled—*i.e.* the curvature of the hanging hairs appears to be greatest in a small region at the bottom of the hairs. The characteristic length l_g of an individual hair (radius r, bending rigidity B, mass density m) determined by a balance between gravity and elasticity is given by $l_g \sim (B/mgr^2)^{1/3} \sim (Er^2/mg)^{1/3}$. For hair that has a natural curvature κ^*, when $l_g\kappa^* \gg 1$, gravity is unimportant, while otherwise gravity does play a role; this can be seen in the variegated forms of human and animal hair and fur. In the case treated here, corresponding to relatively straight hair, the role of gravity is limited to the slight splay seen at the end of the curl seen in Fig. 1b. A more nuanced approach would require us to consider the interactions between elasticity, gravity, natural curvature and packing as treated in ref. 12.

Comparing single helix extension to combing a double helix

To gain insight into the effects of interfilament contact during combing, we compare our force-displacement curves (Fig. 2 and 3) to the curves obtained to stretch out a single helix using the well-known analytic force-extension curves.[18] For a helical filament described by an angle $\alpha \sim P/R$ and helix radius R, and one end clamped, the external load F and torque M applied axially to the helix's free endpoint to deform it to a helix along the same axis with angle α_1 and radius R_1 are

$$F = C\frac{\cos\alpha_1}{R_1}\left(\frac{\sin\alpha_1\cos\alpha_1}{R_1} - \frac{\sin\alpha\cos\alpha}{R}\right) - B\frac{\sin\alpha_1}{R_1}\left(\frac{\cos^2\alpha_1}{R_1} - \frac{\cos^2\alpha}{R}\right) \quad \text{(A1)}$$

$$M = C\sin\alpha_1\left(\frac{\sin\alpha_1\cos\alpha_1}{R_1} - \frac{\sin\alpha\cos\alpha}{R}\right) + B\cos\alpha_1\left(\frac{\cos^2\alpha_1}{R_1} - \frac{\cos^2\alpha}{R}\right) \quad \text{(A2)}$$

Using the geometry of the helix as a function of its end-to-end extension, and assuming that the tine is stuck to the helix when it is inserted into the double helix, we can estimate the force required to stretch the helix, as shown in Fig. 2 and 3, and see that the single-helix force-extension curve vastly overestimates the combing force for a double helix where the tine drives link out of the system as it slides along it.

Varying tine radius

To explore the double-helix parameter space, we varied three dimensionless ratios of length scales: $\pi_1 = P/r$, $\pi_2 = R/r$ and $\pi_3 = t/r$. The effects of varying π_1 and π_2 are shown in Fig. 2 and 3. In Fig. 6, we show the effect of varying π_3. Contrasting Fig. 6 to Fig. 2 and 3, we see that the effect of tine radius on the force required to comb the curl is much smaller than that of the helix pitch or radius.

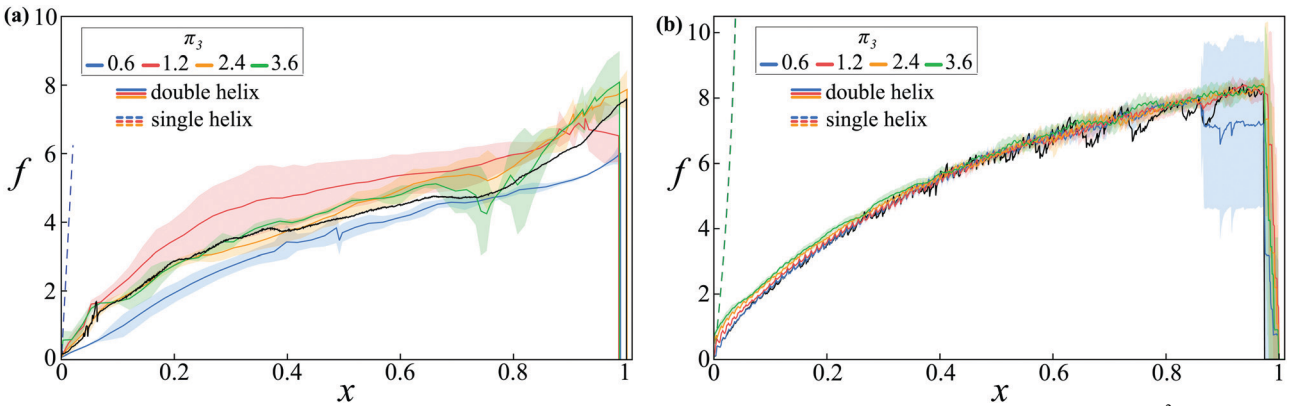

Fig. 6 Force to comb a double helix under variation in tine radius t in (a) experiment and (b) simulation. We show scaled force $f = \frac{l_0^2 F}{B}$ applied by tine over scaled distance combed $x = \frac{d}{D}$, where F is unscaled force, d is unscaled distance combed, l_0 = 0.01m is reference length, B is single filament bending rigidity and D is total tine displacement required to fully unlink the tangle. Dashed curves show theoretical force predicted for stretching single helix an equivalent distance. Black curves show a single representative combing, for $\pi_3 = t/r = 1.2$ in (a) and $\pi_3 = 0.6$ in (b). We vary tine radius relative to hair radius $\pi_3 = t/r$, keeping helix radius $R = r$ and pitch $P = 23.5r$ fixed. Comparing to Fig. 2 and 3, t affects combing force much less than R or P. Note that all combing experiments and simulations in main text used $\pi_3 = 0.9$.

Cost of combing

Before discussing the cost of combing, we define the process of combing in terms of q, the number of pitches in the double helix between the tine insertion point and the free end of the double helix, so that a length-L braid with $q_{tot} = L/P = 1000$ links must be combed through. Combing the long double helix can be achieved *via* a sequence of strokes, each of which detangles q links, or pitches, of the long double helix. For the first combing, the tine is inserted q pitches away from the free end, and is pulled through to the free end, detangling those q links. For each subsequent combing, the tine is inserted q pitches further away from the free end than it was inserted for the previous combing. Each time, it is pulled through to the free end, detangling q new pitches. In all combings after the first one, the tine must push the q pitches through some amount of previously-detangled helix arclength. During this part of the combing, no new links build up in front of the tine; rather, the tine causes the q links to translate down the double helix to the free end.

Our cost function needs to incorporate a measure of the pain associated with the force exerted by the tine, and time spent combing the curl; letting $f_{max} = F_{max}\left(\frac{l_0^2}{B}\right)$ be the maximum dimensionless force felt during combing, we choose the simplest cost that can interpolate between these two contributions:

$$\text{Cost} C(q) = \gamma f_{max} + (1-\gamma)\frac{q_0}{q} \qquad \text{(A3)}$$

where $q_0 = 25$ is a fixed number of pitches characteristic to the q-values used in these combing strategies, and $\gamma \in [0, 1]$ spans possible hair geometries. In particular, as indicated by the force-displacement curves in Fig. 2 and 3, combing curly hair requires more force, hence more pain, while combing straight hair is rather painless. Hence, setting $\gamma = 1$ selects the pain term from the cost and corresponds to combing curly hair, while $\gamma = 0$ chooses the time term and corresponds to combing straight hair. We note that our cost function implicitly incorporates an approximate mechanical work performed in combing the length-L helix using each combing strategy, which can be seen by considering the square of the cost above.

Simulation settings

We model each hair using the Cosserat theory of elastic rods,[24,25] and solve the governing equations using the numerical methods described in earlier work *et al.*[26,27] To simulate large numbers of hairs at once, we parallelize the integration scheme within each timestep, computing forces and torques and updating filament positions, velocities and other quantities for all filaments simultaneously. To parallelize computation of contact forces, we check each filament separately for contact with other filaments, and only update the external forces on individual filaments, avoiding multiple calls to the same memory block by different threads at the same time.

Table 1 Parameters used for estimating real hair crossings

Radius r	7.5×10^{-5} m
Hair length ℓ	0.2 m
E	1 GPa
Poisson ratio ν	0.5
Spatial discretization δl	0.002 m
Time discretization δt	$\left(0.008\frac{s}{m}\right)\delta l$

Table 2 Parameters used for combing nylon double helix

Radius r	4.2×10^{-4} m
Helix height L	0.15 m
Mean E	0.3 GPa
Poisson ratio ν	0.5
Spatial discretization δl	0.014 m
Time discretization δt	$\left(0.08\frac{\text{s}}{\text{m}}\right)\delta l$

We use the simulation and filament parameters listed in Tables 1 and 2, noting that all quantities plotted in this paper are dimensionless, making the real values of E and r used in simulation only representative.

Movie A1

Experimental combing of a double helix. We mold two nylon filaments around a helically-grooved cylinder, forming them into two identical helices that we entwine into a single double helix. We clamp the double helix at one end and let the other end hang freely. This assembly is then pierced at the midpoint of the double helix centerline arclength by a single stiff rod which moves downward to detangle the curl. We use an Instron 5566 material testing machine to measure the force extension curves of a stiff rod piercing and pulling downward on the pinned, hanging helices. Here we show the combing process and corresponding force-displacement curve. The experiment shown is the same as that used to generate Fig. 2e, with $\pi_1 = 18$, $\pi_2 = 1$.

Movie A2

Simulated combing of a double helix. We clamp a double helix at the top allowing it to hang free. We insert a tine halfway down the tangle and gradually displace the tine toward the free end at a constant rate. The simulation proceeds quasi-statically. We show simultaneously a visualization of the combing process, the force-displacement curve and the local change in link density as a function of rescaled arclength s and rescaled tine displacement x. The simulation shown corresponds to the one used to generate Fig. 3e, with $\pi_1 = 18$, $\pi_2 = 1$. See Table 1 for simulation settings.

Acknowledgements

For partial financial support, we thank the National Science Foundation grants NSF DMR 20-11754, NSF DMREF 19-22321, and NSF EFRI 18-30901, and the Henri Seydoux Fund.

References

1 H. M. Gutierrez, J. P. Rust and A.-F. Seyam, *Text. Res. J.*, 1995, **65**, 638–643.
2 M. E. M. Lee and H. Ockendon, *J. Eng. Math.*, 2006, **54**, 261–271.
3 P. Tapadia and S. Wang, *Phys. Rev. Lett.*, 2003, **91**, 198301.
4 L. A. Archer, *J. Rheol.*, 1999, **43**, 1617–1633.
5 D. R. Nelson, *Nature*, 2004, **430**, 839–840.
6 M. A. Berger, *Astron. Astrophys.*, 1991, **252**, 369–376.
7 J. W. S. Hearle and W. E. Morton, *Physical Properties of Textile Fibres*, Elsevier Science & Technology, Cambridge, 2008.
8 N. Pan, *Text. Res. J.*, 1992, **62**, 749–765.
9 A. Panaitescu, G. M. Grason and A. Kudrolli, *Phys. Rev. E*, 2017, **95**, 052503.
10 A. Kabla and L. Mahadevan, *J. R. Soc., Interface*, 2007, **4**, 99–106.
11 G. A. V. Leaf and W. Oxenham, *J. Text. Inst.*, 1981, **72**, 168–175.
12 R. E. Goldstein, P. B. Warren and R. C. Ball, *Phys. Rev. Lett.*, 2012, **108**, 078101.
13 G. Gurtner and M. Durand, *Europhys. Lett.*, 2009, **87**, 24001.
14 J. B. Carleton, G. J. Rodin and M. S. Sacks, *ACS Biomater. Sci. Eng.*, 2017, **3**, 2907–2921.
15 K. Ward, F. Bertails, T.-Y. Kim, S. Marschner, M.-P. Cani and M. Lin, *IEEE Trans. Vis. Comput. Graph.*, 2007, **13**, 213–234.
16 Y. Bao and Y. Qi, *IEEE Access*, 2017, **5**, 12533–12544.
17 P.-G. De Gennes, *Scaling concepts in polymer physics*, Cornell university press, 1979.
18 A. E. H. Love, *A treatise on the mathematical theory of elasticity*, At the University Press, Cambridge [Eng.], 3rd edn, 1920.
19 F. B. Fuller, *Proc. Natl. Acad. Sci. U. S. A.*, 1971, **68**, 815–819.
20 G. C. Călugăreanu, *Rev. Math. Pures Appl.*, 1959, **4**, 5–20.
21 J. H. White, *Am. J. Math.*, 1969, **91**, 693–728.
22 R. L. Ricca and B. Nipoti, *J. Knot Theory Ramif.*, 2011, **20**, 1325–1343.
23 R. Kamien, *Eur. Phys. J. B*, 1998, **1**, 1–4.
24 E. Cosserat and F. Cosserat, *Theorie des Corps Deformables, A. Hermann et Fils*, Paris, France, 1909.
25 O. M. O'Reilly, *Modeling Nonlinear Problems in the Mechanics of Strings and Rods: The Role of the Balance Laws*, Springer International Publishing AG, Cham, 2017.
26 M. Gazzola, L. H. Dudte, A. G. McCormick and L. Mahadevan, *R. Soc. Open Sci.*, 2018, **5**, 171628.
27 N. Charles, M. Gazzola and L. Mahadevan, *Phys. Rev. Lett.*, 2019, **123**, 208003.